Nanometer Scale Scanning Electrochemical Microscopy Instrumentation

Jiyeon Kim, Christophe Renault, Nikoloz Nioradze, Netzahualcóyotl Arroyo-Currás, Kevin C. Leonard*, and Allen J. Bard*

Supporting information

Table of Contents

1. Experimental

Chemicals and Materials. Ferrocenyl methyl trimetylammonium iodide ($FcTMA^+$ I^-), perchloric acid and sodium perchlorate were purchased from Sigma Aldrich and used as received. Ferrocenyl methyl trimethylammonium perchlorate ($FcTMA^+$ ClO_4^-) was prepared by metathesis. Hydrochloric acid, hydrogen peroxide and sulfuric acid were obtained from Fisher Scientific and used as received. For the electrodeposition of Pt nanoparticles, hexachloroplatinate solution (8 wt % H_2PtCl_6 in H_2O) was purchased from Sigma Aldrich, and HOPG (ZYB grade, Micromasch) was used after a fresh cleavage. A Milli-Q Integral system (Integral 5, EDM Millipore, Berllerica, MA) was equipped to obtain ultrapure water with total organic carbon (TOC) level at < 3 ppb as measured by an internally equipped TOC monitor as well as the resistivity 18.3 MΩ-cm. All the solutions for electrochemical measurement were prepared with ultrapure water and filtrated using a syringe filter with 100 nm diameter pore (Millex-Syringe driven filter unit, PVDF-0.1 μm, Merck Millipore Ltd.) except the acidic solution. All the glassware and the SECM cell made of Teflon and glass were extensively cleaned with piranha solution (1:1 ratio of H_2SO_4 : H_2O_2) followed by thorough washing with ultrapure water before use to protect their surface from airborne contaminants prior to performing SECM measurements.

Pt nanoelectrode fabrication. Pt nanoelectrodes were fabricated by using a CO_2-laser puller, microforge and a focused ion beam (FIB) instrument as reported elsewhere.[S1] Briefly, 25 μm dia. Pt wire (Goodfellow, annealed) inserted in the borosilicate capillary (I.D. 0.2 mm, O.D. 1mm, item No 9-000-2000, Drummond scientific company, Broomall, PA) was pulled together with CO_2 laser puller (P-2000, Sutter). Continuously, Pt nanoelectrode was further annealed by

microforge (MF-0P, Narishige, Japan) for a smaller RG (a ratio between glass sheath and Pt radii) as well as a better sealing. The annealed Pt UME was milled by FIB (FEI Strata™ DB235) to expose Pt disk resulting in an inlaid disk shaped electrode with nanometer level smoothness. To avoid any damage of electrode caused by electrostatic discharge, we handled Pt nanoelectrode with protection tools.[S2] Prepared Pt nanoelectrode was also used under 30 % or higher relative humidity at 22~23 °C.

Electrodeposition of Pt NPs on HOPG. A detailed information and procedure are reported elsewhere.[S3] Briefly, A CHI760E bipotentiostat (CH Instrument, Austin, TX) was used for the electrodeposition of Pt NPs with a three electrode cell configuration, where HOPG, mercury sulfate electrode (MSE) and Pt disk electrode are working, reference and counter electrodes, respectively. First, freshly cleaved HOPG was prepared. Before immersing HOPG in the plating solution containing 1 mM H_2PtCl_6, 0.1M HCl, a constant potential at 0.27 V was held to HOPG from the air to the plating solution (or vise versa) to avoid a spontaneous deposition of Pt on HOPG.[S4] Using a multiple potential step technique, a constant potential of −0.6 V vs MSE was applied to HOPG during electrodeposition for 240 s. After electrodeposition, the potential returned to the initial potential, 0.27 V to completely stop the deposition process. For this potential control, "return to the initial potential after run" function was activated in the CHI software. To avoid damages by electrostatic discharge on either Pt NPs or HOPG, we handled HOPG with protection tools as well as using the "cell on between run" function as reported elsewhere.s[2] Also, the relative humidity was maintained over 30 % at 22~24 °C. Once Pt NPs/HOPG was prepared, it was stored in ultrapure DI water in the closed cell to protect its surface from airborne contaminants before performing SECM measurements.

Overall Operation and Procedures. CHI760E bipotentiostat (CH Instrument, Austin, TX) was employed for electrochemical control. Particularly, all relay switches for working electrode 1 (WE1), working electrode 2 (WE2), reference electrode (RE) and counter electrode (CE) in CHI760E bipotentiostat were physically removed by following manufacturer's instruction to avoid electrochemical damage of nanometer sized Pt nanoelectrode during SECM measurements (detailed information is in the main text). For the electrochemistry, a four electrode cell configuration was used with two Pt wires as quasi reference (QRE) and counter electrodes. The electrochemistry was operated by CHI software using the "cell on between run" function since there are still other relays to be controlled properly, where both the nano tip (Pt nanoelectrode) and the substrate (HOPG) currents were recorded during the entire experiments. Simultaneously, the piezo was operated by the LabView code with reading the analog output signal (current) from the CHI760E bipotentiostat through data acquisition board (USB-6009 Multifunction I/O, National Instrument), thus synchronizing the movement of piezoelectric actuators with the corresponding tip current as a function of distance between the nano tip and the substrate. For the proper connection of the nano tip under "cell on between run function", dummy voltammetry was run under RE and CE connection in the presence of electrolyte prior to connecting tip (WE1) or HOPG (WE2). To suppress the local thermal drift, the electrochemical cell was covered with a lid to avoid solvent evaporation during the experiment.[S5] To suppress any electrode damage due to ESD, we handled Pt UME and HOPG with protection tools as reported elsewhere.[S2] Also, the relative humidity was maintained over 30 % at 22~24 °C.

SECM procedures and measurement. Firstly, PIMikroMove (PI) was used to control the drift compensation mode to eliminate drift in the digital-analog converters on the E-816 submodule

plugged into the main board of the controller. A Pt nanoelectrode as an SECM tip was then positioned c.a. 100 μm above the HOPG substrate with a lockable micropositioner in z axis under the video microscope, then micropositioners were locked. Continuously, the tip was brought closer to the substrate by the SECM approach curve technique until the feedback current appeared in the presence of either $FcTMA^+$ or H^+ in the electrolyte solution (details about solution composition and potentials at the nanotip and the substrate are described below). When the z-piezoelectric actuator reached the limit of its travel distance (c.a. 50 μm) before showing any feedback current response, the z-piezo was completely contracted and the nanotip was manually lowered down with a micropositioner at 40 μm distance after unlocking. Then, the manipulator was locked again and the nanotip was approached with z-piezo at 50 nm/s (5 nm/0.1 s) rate by SECM approach technique until feedback appeared. After 2 to 3 times of this repetitive procedure as described above, the nanotip can be positioned c.a. 20 μm above the substrate, where the z-piezoelectric actuator has enough room to expand. The fine current-distance curves were obtained at 10 nm/s (1 nm/0.1 s) rate for the subsequent fine approach. This rate is important not only for the prompt controlling of the tip position to avoid tip crash over the substrate but also for the sufficient equilibrium time for a piezo actuator to minimize an additional creeping. Once the nano tip approached to within a feedback distance comparable to the radius of the tip, then the tip approach was stopped and held. At the fixed distance, the tip current was kept monitored. A stable tip current level was confirmed, thus forming a stable nanogap between the tip and substrate with a drift level < 0.5 nm/min (see Figure 3b). Subsequently, the constant-height SECM images were obtained at 200 nm/s (incremental distance 20 nm per incremental time 0.1 s). To get the constant-height SECM image based on H^+ reduction/H_2 oxidation, –1.0 V and –0.4 V vs Pt QRE were applied to the tip and Pt NP/HOPG,

respectively, where H^+ was reduced at the nanotip and tip generated H_2 was oxidized at the Pt NPs on HOPG substrate. Specifically, –0.4 V vs Pt QRE for HOPG substrate is chosen to prevent the Pt oxide formation. In the same way, the SECM imaging was conducted in the electrolyte solution containing 1 mM $FcTMA^+$, 10 mM $NaClO_4$ and 0.3 V and –0.1 V vs Pt QRE were applied to the nanotip and Pt NP/HOPG substrate, respectively, where $FcTMA^+$ was oxidized at the nanotip and tip generated $FcTMA^{2+}$ was reduced at the substrate with diffusion controlled rates. All experiments were carried out in the isothermal chamber at a relative humidity maintained over 30 % at 22 °C. (More details about electrochemical study are reported elsewhere.[S3])

2. LabVIEW Code

National Instrument's LabVIEW was used to create the software to interface and synchronize the tip motion with the measured tip current from the bi-potentiostat, similar to what Leonard and co-workers previously reported.[S6] Figure S1 (Supporting Information) shows a schematic of the LabVIEW block diagram used to code the SECM mapping technique. The data acquisition of the analog output signal from the bi-potentiostat (top section of Figure S1), and the motion-control of the piezos (bottom section of Figure S1) were performed in parallel using nested for-loop architecture. Prior to starting the nested for-loop, the data acquisition device was initialized and set to measure an analog input (AI) signal using National Instruments' DAQmx driver. The piezo was initialized using a custom initialization subVI (PI Init), which called Physik Instrumente's LabVIEW driver. The nested for-loop structure allows for the tip to be raster-scanned across the substrate. The interior for-loop steps the piezo in the x-direction for a set number of steps, and upon completion of the interior for-loop, the piezo performs one step in

the *y*-direction and moves the piezo back to the initial *x* position. All custom subVIs that control the motion of the piezos internally call the Physik Instrumente's LabVIEW driver. An advantage of developing our own custom subVIs, combined with the modularity of LabVIEW, is that it allows for different motion-control manufacturers to be utilized, if necessary, by simply changing which LabVIEW driver is called inside this custom subVIs.

The SECM mapping program proceeds as follows. At the beginning of the interior for-loop, the custom subVI PI Step is called, which moves the piezo in the x-direction with a distance given by the "step increment" variable. After the piezo is stepped, its exact position is read using the PI Read subVI. In parallel, the voltage from the analog output signal is read via the DAQmx Read subVI at a sampling rate set by the DAQmx Sample Clock subVI. The tip electrode is then held in position for a duration dictated by the variable "step time," while the multiple voltage readings are collected. These voltage readings are then multiplied by the "tip current range" variable, which is set in the CH software, to convert the voltage reading to measured currents. These measurements are averaged to reduce sample noise and to produce a single current value at the given tip position. The tip position and measured tip current are entered into a custom 3D Plot subVI which creates a 3D image of the x-y scan with colors representing tip currents. The timing of the interior for-loop is driven by LabVIEWs internal "Wait Until Next Milli-second Multiple" subVI, which forces each iteration of the for-loop to start on equal spaced intervals dictated by the "step time" variable. After the tip is moved back to the starting x-position in the external for-loop, a delay was added to reduce any tip current artifacts that are produced due to convection caused by quickly moving the SECM tip a large distance. Upon completion of the nested for-loops the connection to the data acquisition device and piezo is closed, and the tip current versus position data is saved to file. The algorithm used to

approach the tip to the substrate and generate approach curves, is similar to what is shown in Figure S1, with the exceptions that only a single for-loop is used and the piezo is stepped in the z-direction (shown in Figure S2). Additional LabVIEW code (shown in Figure S3) was also used to update the graphical user interface in real time as either the mapping or approach curve experiment was occurring.

The VIs we provide here are "dummy" VIs which show how to do the motion control, but do not actually contain PIs driver we used. We shared this generic version of VIs so the users could use any manufacture (PI, Newport, etc.) and just replace our "dummy" VIs with the manufacture that they chose to use.

2.1 LabVIEW Code for Mapping.

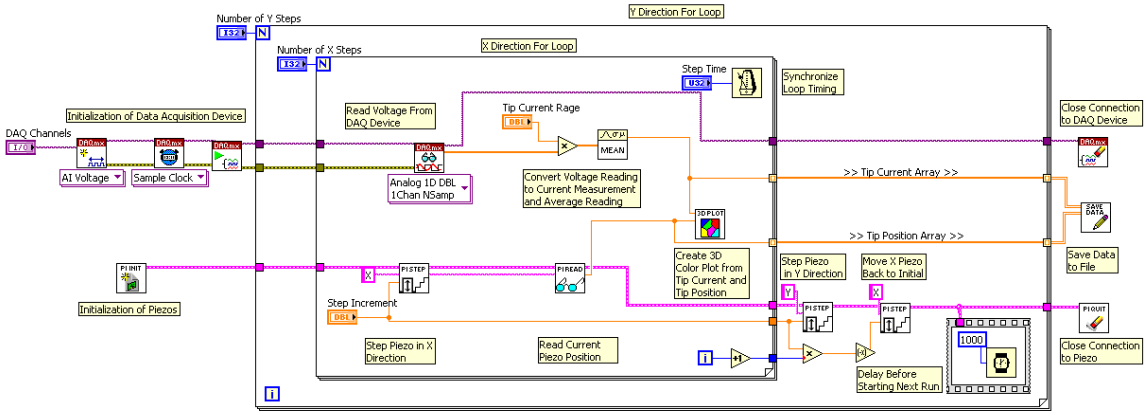

Figure S1. A schematic of the LabVIEW block diagram showing the nested for-loop architecture with the data acquisition and piezo motion control occurring in parallel. (Larger image and actual VI file are available on the ACS Publications website).

2.2 LabVIEW Code for Approach Curves.

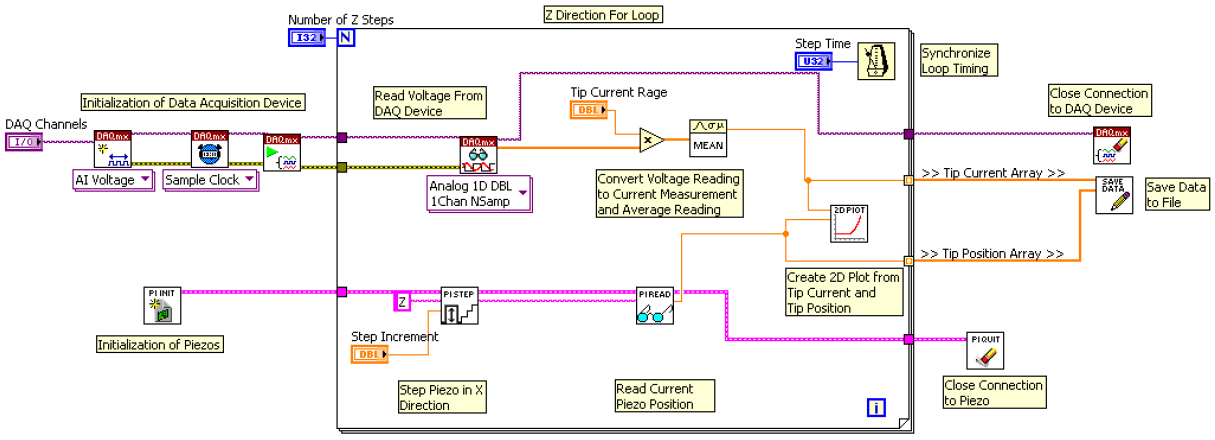

Figure S2. A schematic of the LabVIEW block diagram showing the single for-loop architecture with the data acquisition and piezo motion control occurring in parallel used to obtain approach curves (Larger image and actual VI file are available on the ACS Publications website).

2.3 LabVIEW Code for Graphical Interface.

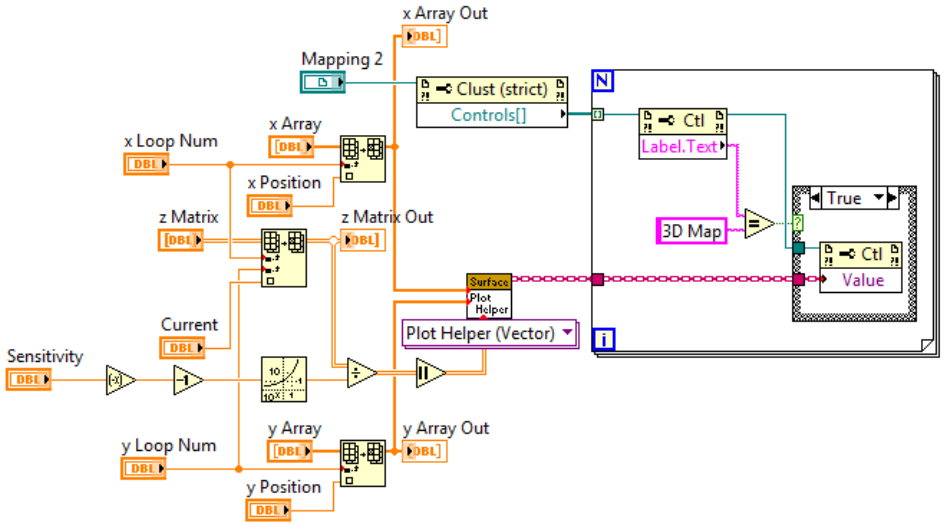

Figure S3. A schematic of the LabVIEW block diagram showing the architecture to create the 3D plot data and display the data in real time on the user interface. (Larger image and actual VI file are available on the ACS Publications website).

3. Pictures of CHI760E bipotentiostat board before and after removing relay switches

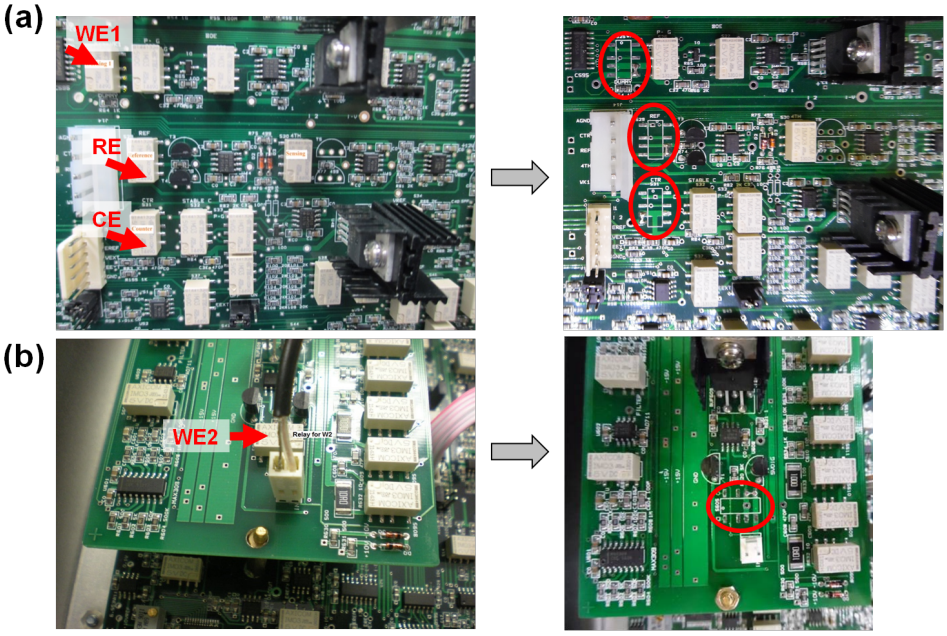

Figure S4. (a, b) Pictures of CHI760E bipotentiostat board before (left) and after (right) removing relay switches. WE1, RE, CE, and WE2 represents working 1, reference, counter, and working 2 electrodes. Each relay switch for the corresponding electrodes is denoted with red arrows. After removing relay switches, we short "common" and "normal open" connections represented with open circles.

We confirm the intactness of a Pt tip by scanning electron microscopy after SECM experiment with above relay switch-removed bipotentiostat This tip was used at applied tip and substrate potentials, E_{tip} = 0.3 V and $E_{substrate}$ = −0.1 V vs Pt QRE, respectively. Note that our SECM operation doesn't include the swapping of WE1 and WE2, thus such a particular operation may need a different modification to protect the tip from the electrochemical damage.

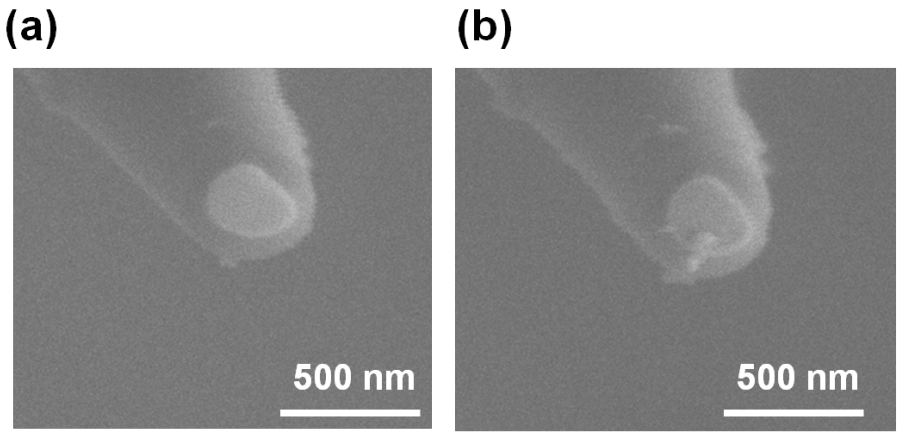

Figure S5. (a, b) SEM images before (left) and after (right) SECM experiments with a relay switch-removed bipotentiostat, where tip-substrate potential difference is 400 mV. Pt disk remains intact after the SECM experiment with the biased substrate.

4. The Construction of the Isothermal Chamber

We constructed isothermal chamber as reported elsewhere[S5]. In this work, we constructed an isothermal chamber made with Polystyrene foam (Lightweight Polystyrene Foam Insulation, 48" × 48" × 2", High Density, 9255K3, McMaster Carr). The overall dimension is 8'(*l*) × 6'(*w*) × 8' (*h*) with a door as depicted in Figure S6a. Polystyrene foams were stacked and connected to directly face to each foam and the connection was made on the outside of the foam using industrial double sided Velcro tapes (Velcro brand Industrial Strength, 2" ×15', Amazon.com). The inherently sharp edge of the polystyrene foam was used to seal the gap between the foam plates, thus minimize the airflow though the gap. No additional sealing was made on the constructed plates.

In the chamber, the entire vibration isolation table with faraday cage (30" × 36" × 6') including SECM stage was placed. Since a vibration isolation table is mainly made with stainless steel, it was intended to act as a heat sink as mentioned in Amemiya's previous work[S5]. In fact, the larger dimension of an isothermal chamber and the big enough air space surrounding the

vibration isolation table can be less sensitive to the local thermal drift, thus more advantageous to make an isothermal condition. Herein, we didn't monitor the temperature in this chamber. All evaluation of the isothermal capability of the chamber was made based on the tip position drift as shown in Figure 2. Generally, it takes 40 min to approach the nanometer sized tip within the feedback range (c.a. comparable size of tip radius) over the substrate and monitor the tip current as a measure of tip positional drift. The characteristic result in Figure 2 was obtained about 50 min after the tip was initially placed on the tip holder mounted on the SECM stage and 2~3 time repetitive procedures to manually control the micropositioner mentioned in section 1, SECM procedure. So, the temperature becomes stabilized within 20 min after the isotheral chamber was opened / closed. In Figure S6, a schematic view and the pictures of the isothermal chamber are shown.

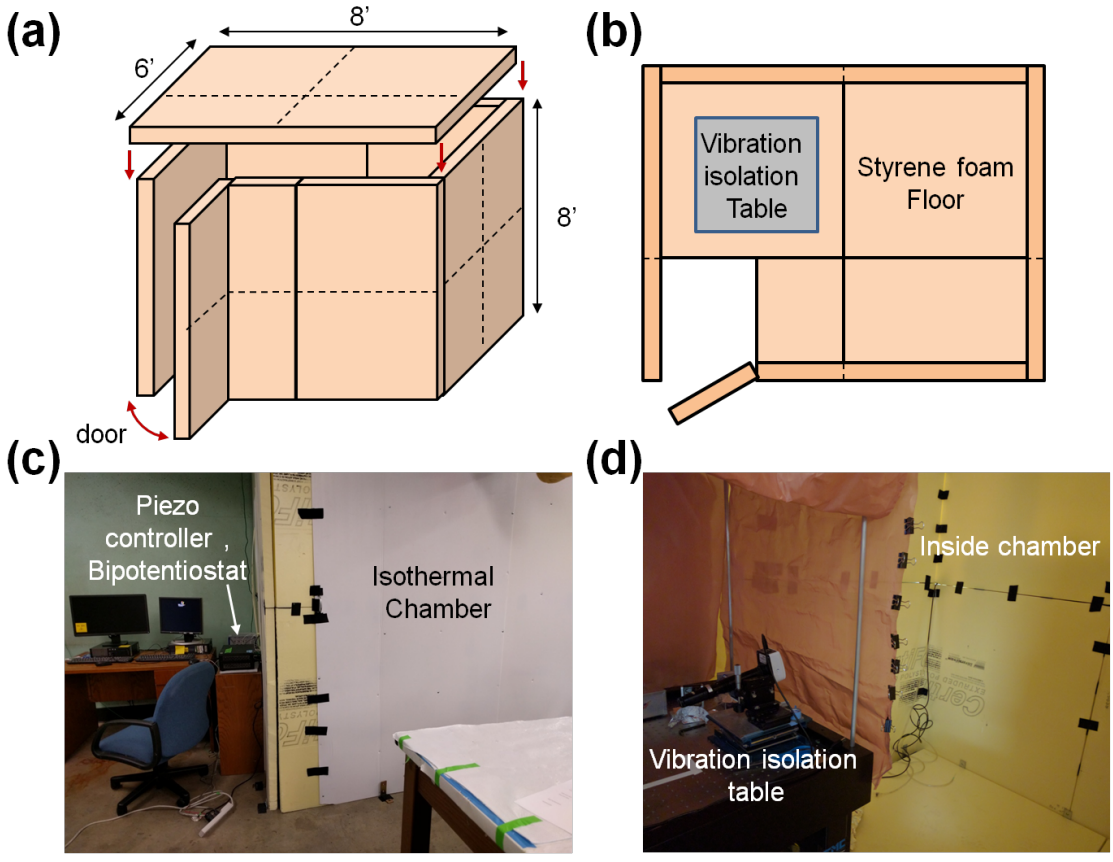

Figure S6. (a) The schematic view of overall dimensions in the isothermal chamber. (b) Top view of the isothermal chamber inside. Entire vibration isolation table with SECM stage is placed in the isothermal chamber. (c) (d) pictures of the isothermal chamber outside and inside.

5. Amperometric Current Response in the Bulk Solution vs Over the Substrate.

When we monitored the current transient in the bulk $FcTMA^+$ solution at E_{tip} = 0.35 V vs Pt QRE with time, the overall current change was less than 2 % compared to the initial steady state current as shown in Figure S7a. Such a stable current response could be obtained under the highly purified condition with nanopure water, freshly synthesized $FcTMA^+$, a piranha cleaned electrochemical cell and a lid for the electrochemical cell for a minimum exposure to the air. Under this controlled condition of contamination, the tip current response stably maintains free from usual tip fouling. Owing to the stable current response, the tip positioning drift could be clearly differentiated from the general tip fouling caused by the adsorption of redox mediator or any impurity. Recently, Unwin and co-workers reported an adsorption of redox mediator on the HOPG surface during their SECM experiment.[S7] However, it could have a much stronger adsorption effect due to their inherent experimental setup such as small droplet based electrochemical cell, where the solvent evaporation might cause much stronger adsorption of redox mediators on the tip surface. Compared to that, we haven't seen any strong effect of adsorption of redox mediator on the tip, thus the tip current responses was stable during the SECM experiment, which allowed us to do quantitative measurements in nanoSECM. This result is also consistent with Amemiya's recent work on the graphene or HOPG surface, where the adsorption effect was negligibly observed.[S8,S9] As long as the contamination is well controlled,

Using the redox mediator to measure tip-substrate distance is not a backward step but straightforward to make nm level tip positioning.

In the magnified the current transient obtained in the bulk, we could observe the current fluctuation of the maximum 2 % (Figure S7b). This fluctuation might be attributed to the gradual convection of solution or a fluctuation of applied potential or both. In fact, the present bipotentiostat (CHI760E) has accuracy of applied potential, ± 1 mV. So far, we don't have any control of a solution convection.

The tip positioning drift induced by the thermal drift has a monotonic change, thus we extracted the overall tip drift over the time from the moment (300s in Figure S7c) when tip stopped approaching and was held over the insulating substrate to the time point (900s) before the tip was withdrawn from the substrate. In Figure S7c, the overall tip current change from 300 s to 900 s is almost negligible, implying stable tip position over the substrate. The fluctuation in current in this time range is about 2 %, which is consistent level observed in the bulk solution.

In the isothermal chamber, we could reproducibly get the drift level smaller than 0.5 nm/ min up to 0.1 nm/min. Since we directly converted the current change to the tip displacement over the substrate by using the reverse function of approach curve, any fluctuation in current could be resulted in the tip displacement. The stability of piezo itself is ± 1 nm as reported by the manufacture (Physik Instrumente, http://www.pi-usa.us/products/PDF_Data/P620_2_Precision_Piezo_Nano-Positioning-Stage.pdf).

If this current fluctuation was caused by piezo fluctuation at ± 5 nm level, we could've seen extremely fluctuating current response over the nanoparticle since the working distance is only 14 nm over the apex of nanoparticle. We didn't observe such a behavior. Considering all, the current fluctuation at 2 % level in the tip drift test could be attributed to the potential

fluctuation in the bipotentiostat or gradual solution convection or both instead of the piezo fluctuation of ± 5 nm.

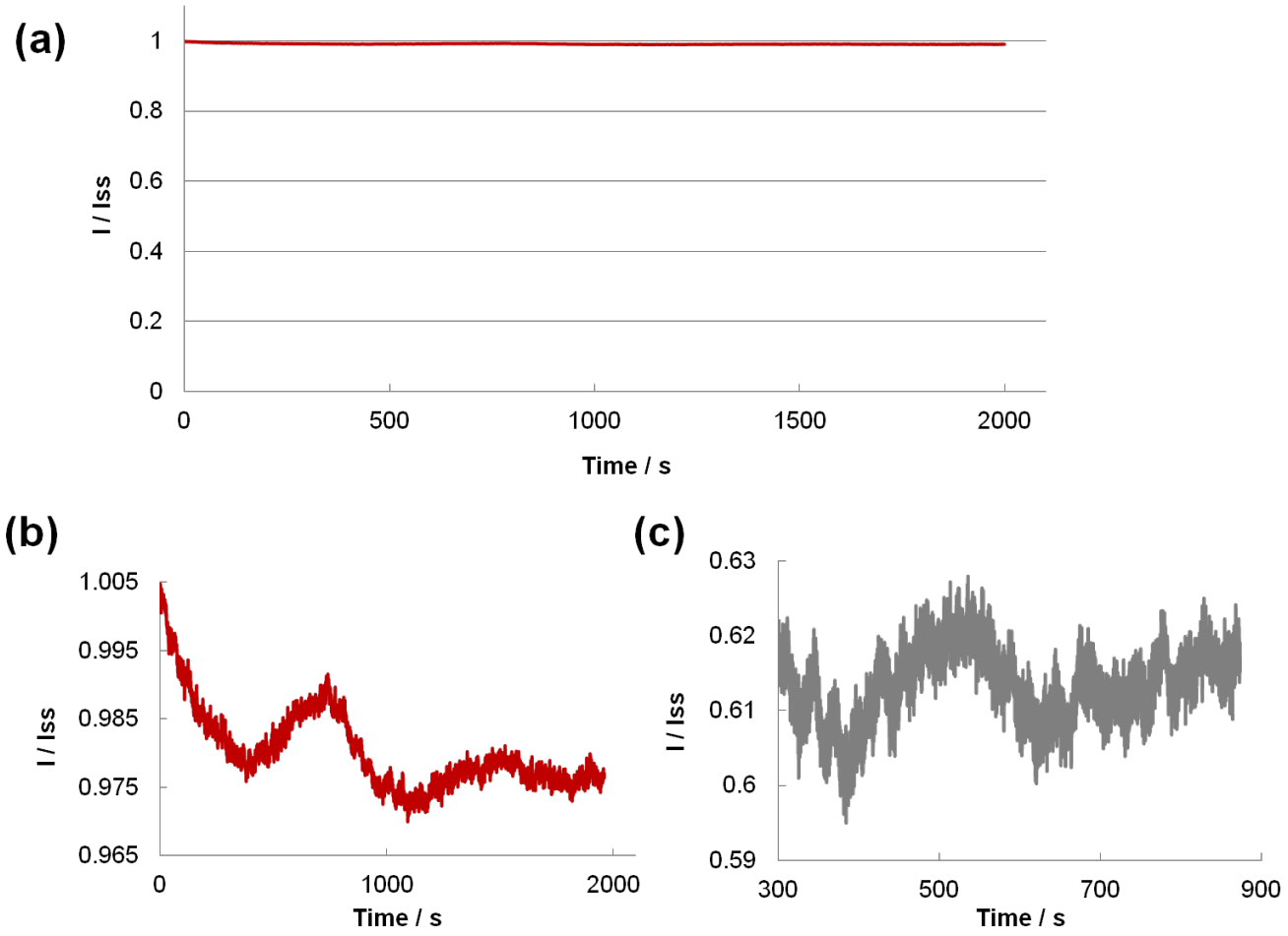

Figure S7. (a) The tip current transient in the bulk $FcTMA^+$ solution at E = 0.35 V vs Pt QRE. The current is normalized against the initial steady state current. (b) The magnified current response from panel a (in the bulk). The overall current change is less than 2 %. Also, fluctuations in current at 2 % level are observed. (c) The magnified current response from Figure 2b (normalized original amperometric data of Figure 3b, over the insulating substrate). At 300s in this plot, tip stopped approaching and held over the insulating substrate while the current was monitored until the tip was fully withdrawn to bulk at 900 s. The overall tip current change from 300 s to 900 s is almost negligible, implying stable tip position over the substrate. The fluctuation in current in this time range is about 2 %, which is consistent level observed in the bulk solution.

5. SECM image in Figure 6 and Theoretical Fitting.

The lateral drift during imaging is caused by instability of tip position due to the unlockable micropositioner. During the tip scanning in x and y axes, it is not obvious to measure the accurate drift in lateral tip position since there could be a combinational influence from both x and y-axis micropositioners at the same time. The most straightforward way to measure the instability of each unlockable micropositioner could be the tip drift test in z-axis over the substrate by mounting them to z-axis. Such an inherent instability could subsequently depend on the mounting direction of micropositioners from right to left (or vise versa), from forward to backward (or vise versa) during the imaging because the drift could be on the same direction as or opposite direction to tip scanning direction. Surely, tests with several combinations could be performed, which is negative experiment and beyond our interest. In fact, the ellipsoidal shaped image implies that the lateral drift during imaging is not a monotonic change such as thermal drift. If so, we could have observed an entirely shifted position of images instead of a deformed image with different aspect ratio.

Still, we can approximately evaluate the apparent level of lateral drift comparing the experimental data and simulation data. Under 200 nm/s scan rate (20 nm incremental distance per 0.1 s incremental time), we could see about 59 nm discrepancies in half peak width in 1 s in Figure 5c. This 59 nm/s level of nonmonotonic drifts is significant enough to deform the SECM image and cause the artifact.

Once we replaced all unlockable micropositioners with lockable ones, we could perform an SECM image in 1 mM $FcTMA^+$ solution with a 90 nm radius Pt tip. The resulting SECM image is shown in Figure 6 as a raw data. The image was obtained at 200 nm/s scan rate (20 nm

incremental distance per 0.1 s incremental time). Overall, it took 7 min to get 1.2 × 1.2 μm^2 image (x is long scanning axes, additional 1 s waiting at each $x = 0$ to avoid any transient effect on SECM image). Figure 6a was plotted with Image *J* software provided by NIH with following parameters; filled mode, Thermal LUT color, Grid size 256, smoothing 0.0, perspective 0.0, Lighting 0.2, max 100 %, min 26 % for better contrasts. In Figure 6b, we showed the fitting of the line scan data at y=0.4 μm from Figure 6a with theoretical data (90 nm radius Pt tip, 120 nm radius and 120 nm height Pt NP) under the diffusion controlled condition at the constant height 72 nm using a finite element analysis with COMSOL Multiphysics. The good agreement between two data sets verified the successful suppression of the lateral tip position with lockable micropositiners. More significantly, this result unambiguously proves that a single NP was imaged by SECM.

References

S1 . Kim, J.; Izadyar, A.; Nioradze, N.; Amemiya, S., *J. Am. Chem. Soc.*, **2013**, 135, 2321-2329.

S2. Nioradze, N.; Chen, R.; Kim, J.; Shen, M.; Santhosh, P.; Amemiya, S., *Anal. Chem.*, **2013**, 85, 6198-6202.

S3 . Kim, J.; Renault, C.; Arroyo-Currás, N.; Nioradze, N.; Leonard, K. C.; Bard, A. J., *J. Am. Chem. Soc.*, **2016**, 138, 8560-8568.

S4 . Zoval, J. V.; Lee, J.; Gorer, S.; Penner, R. M., *J. Phys. Chem. B.*, **1998**, 102, 1166-1175.

S5 . Kim, J.; Shen, M.; Nioradze, N.; Amemiya, S., *Anal. Chem.*, **2012**, 84, 3489-3492.

S6 . Barforoush, J.M.; McDonald, T.D.; Desai, T.; Widrig, D.; Bayer, C.; Brown, M. K.; Cumming, L.C. and Leonard, K.C. *Electrochim. Acta,* **2016**, 190, 713-719.

S7 . Tan, S-Y.; Zhang, J.; Bond, A. M.; Macpherson, J.; Unwin, P. R., *Anal. Chem.*, **2016**, 88, 3272-3280.

S8 . Nioradze, N.; Chen, R.; Kurapati, N.; Khcataeva-Domanov, A.; Mabic, S.; Amemiya, S., *Anal. Chem.*, **2015**, 87, 4836-4843.

S9 . Chen, R.; Nioradze, N.; Santhosh, P.; Li, Z.; Surwade, Su.; Shenoy, G. J.; Parobek, D. G.; Kim, M. A.; Liu, H.; Amemiya, S., *Angew. Chem. Int. Ed.*, **2015**, 54, 15134-15137.